ACS APPLIED MATERIALS & INTERFACES

Research Article

www.acsami.org

Decomposition of Organometal Halide Perovskite Films on Zinc Oxide Nanoparticles

Yuanhang Cheng,[†] Qing-Dan Yang,[†] Jingyang Xiao,[‡] Qifan Xue,[‡] Ho-Wa Li,[†] Zhiqiang Guan,[†] Hin-Lap Yip,[‡] and Sai-Wing Tsang*[,†]

[†]Department of Physics and Materials Science, City University of Hong Kong, Hong Kong SAR, P. R. China

[‡]Institute of Polymer Optoelectronic Materials and Devices, State Key Laboratory of Luminescent Materials and Devices, South China University of Technology, Guangzhou 510640, P. R. China

Supporting Information

ABSTRACT: Solution processed zinc oxide (ZnO) nanoparticles (NPs) with excellent electron transport properties and a low-temperature process is a viable candidate to replace titanium dioxide (TiO_2) as electron transport layer to develop high-efficiency perovskite solar cells on flexible substrates. However, the number of reported high-performance perovskite solar cells using ZnO-NPs is still limited. Here we report a detailed investigation on the chemistry and crystal growth of $CH_3NH_3PbI_3$ perovskite on ZnO-NP thin films. We find that the perovskite films would severely decompose into PbI_2 upon thermal annealing on the bare ZnO-NP surface. X-ray photoelectron spectroscopy (XPS) results show that the hydroxide groups on the ZnO-NP surface accelerate the decomposition of the perovskite films. To reduce the decomposition, we introduce a buffer layer in between the ZnO-NPs and perovskite layers. We find that a commonly used buffer layer with small molecule [6,6]-phenyl-C61-butyric acid methyl ester ($PC_{61}BM$) can slow down but cannot completely avoid the decomposition. On the other hand, a polymeric buffer layer using poly(ethylenimine) (PEI) can effectively separate the ZnO-NPs and perovskite, which allows larger crystal formation with thermal annealing. The power conversion efficiencies of perovskite photovoltaic cells are significantly increased from 6.4% to 10.2% by replacing $PC_{61}BM$ with PEI as the buffer layer.

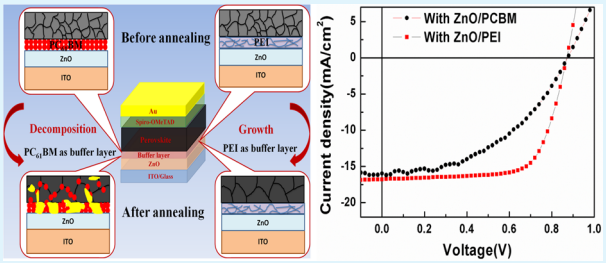

KEYWORDS: *zinc oxide nanoparticles, perovskite solar cell, decomposition, buffer layer, poly(ethylenimine)*

1. INTRODUCTION

Since the first report of an organometal halide perovskite ($CH_3NH_3PbI_3$) sensitized solar cell by Miyasaka et al.,[1] perovskite solar cells have attracted considerable attention due to their excellent optoelectronic properties, ease of solution fabrication process, and remarkable photovoltaic performance. In 2012, Kim et al. demonstrated an all-solid-state perovskite solar cell with promising power conversion efficiency (PCE) by optimizing the device structure and perovskite film morphology and crystallinity.[2] This all-solid-state device structure has become the prototypical device architecture for the development of perovskite solar cells during the past few years; the highest certified PCE of perovskite solar cell has already achieved 20.1%.[3] So far, the most efficient perovskite solar cells with PCE over 15% have a typical structure of anode/HTL/perovskite/ETL/cathode, where HTL and ETL are the hole and electron transporting layers, respectively.[4−7] The HTL and ETL not only play roles in controlling the hole and electron currents, but also in preventing the perovskite active layer from direct contact with the electrodes to reduce recombination of photocurrent.[8] For example, a conducting polymer poly(3,4-ethylenedioxythiophene):polystyrenesulfonate (PEDOT:PSS) is a commonly used HTL in recently developed perovskite solar cells. However, it is well-known that the high acidity of PEDOT:PSS would cause corrosion of the ITO electrode and its high hygroscopicity would absorb water molecules and accelerate device degradation.[9] Consequently, it has been reported that PEDOT:PSS has a detrimental effect on the long-term stability in organic electronic devices.[10,11] Recently, a lot of effort has been devoted to developing different interlayer materials for high-efficiency perovskite solar cells. Over 15% PCE of perovskite solar cells has been demonstrated with polymeric hole transporting materials, such as poly[*N*,*N*′-bis(4-butylphenyl)-*N*,*N*′-bis(phenyl)-benzidine] (poly-TPD) and poly(triarylamine) (PTAA),[9,12] and inorganic hole transporting materials, such as CuSCN and NiO.[13,14] Regarding the electron transporting materials, more robust and stable metal oxide based ETLs have been developed for perovskite solar cells, such as titanium dioxide (TiO_2),[15,16] zinc oxide (ZnO),[17] and tin oxide (SnO_2).[18] Among the metal oxides, TiO_2-NPs have been widely used as ETLs to facilitate charge collection.[15,16] However, in order to obtain the conductive (anatase) phase

Received: May 29, 2015
Accepted: August 17, 2015
Published: August 17, 2015

DOI: 10.1021/acsami.5b04695
ACS Appl. Mater. Interfaces 2015, 7, 19986−19993

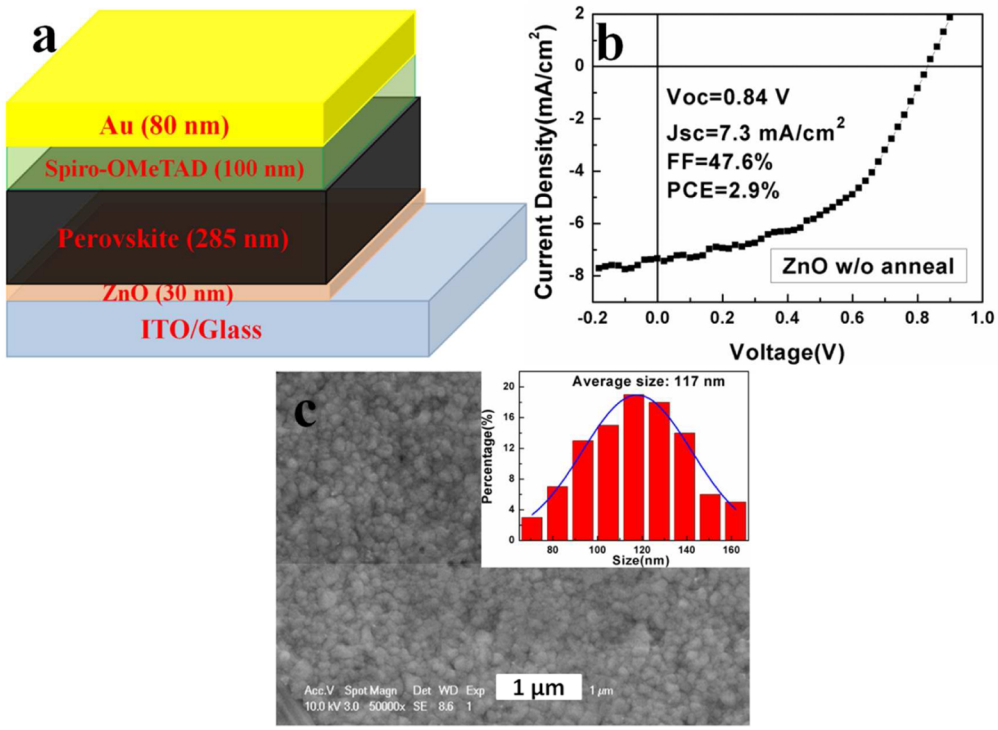

Figure 1. (a) Device structure of ZnO based perovskite solar cell, (b) current density−voltage (J−V) curve of perovskite solar cell based on ZnO without thermal annealing, and (c) SEM image and grain size distribution of perovskite film (without thermal annealing) deposited on ZnO (without thermal annealing).

of TiO_2-NPs, a high sintering temperature (450−500 °C) is required.[19] This is not suitable to be used with ITO where the indium would diffuse out over 300 °C. More importantly, such a high temperature also hinders the development of perovskite solar cells on low-cost flexible plastic substrates.

Recently, solution processed colloidal ZnO-NPs have been applied in the development of several thin film photovoltaic technologies.[20−22] Compared to TiO_2, due to the ability of as-synthesized ZnO-NPs to be processed at room temperature without additional annealing treatment, ZnO-NPs are an excellent candidate to replace TiO_2 used as the ETL in perovskite solar cells.[23] In addition, there are also several reports on organic photovoltaic cells with record high PCE using ZnO-NPs.[24,25] However, there are only a few reports of perovskite solar cells using ZnO-NPs as the ETL. Interestingly, the ZnO-NP based perovskite solar cells have PCE generally lower than that of TiO_2; even both metal oxides have very similar optoelectronic properties. Moreover, the reported perovskite solar cells with ZnO as the ETL typically used lower annealing temperature and shorter annealing time to anneal the perovskite thin films than that (80−100 °C, 30−60 min) typically used in other reported device structures.[26−29] For example, Dong et al.[17] reported a PCE of 8.5% for ZnO nanorod based perovskite solar cell with annealing temperature of 90 °C for 5 min. Kumar et al.[30] demonstrated a PCE of 8.9% with perovskite film annealed at 70 °C on ZnO nanorods. Son et al.[31] compared the photovoltaic performance of perovskite solar cells on ZnO nanorods with that of TiO_2 nanorods: they found the ZnO nanorods had more effective charge collection properties than those of TiO_2 nanorod based perovskite solar cells, and they obtained a PCE of 11% by annealing the perovskite film at 100 °C for 10 min. Therefore, we speculate that there are limitations of using ZnO as the ETL in perovskite solar cells requiring that only low annealing temperature and short annealing time can be used, which limit the perovskite crystal growth as well as the photovoltaic performance.

In this work, we have systematically investigated the application of ZnO-NPs as the ETL on the performance of $CH_3NH_3PbI_3$ perovskite solar cells. Plausibly, we have found that $CH_3NH_3PbI_3$ crystal will severely decompose into PbI_2 during the annealing process if the perovskite film is directly contacted with the ZnO layer. We have shown that, for the first time, the origin of such decomposition of the perovskite crystal on ZnO-NPs is due to the hydroxide constitutions on the as-synthesized ZnO-NP surface. In order to avoid direct interaction between the ZnO and perovskite thin films, two different buffer layers of [6,6]-phenyl-C61-butyric acid methyl ester ($PC_{61}BM$) and poly(ethylenimine) (PEI) have been deposited in between the perovskite and ZnO layers. We have found that PEI can effectively separate the two layers without notable decomposition in perovskite even annealed at 100 °C for 1 h. The ZnO-NP based perovskite solar cell with PEI as the buffer layer achieved a PCE of 10.2% with fill factor as high as 69.0%.

2. EXPERIMENTAL SECTION

Materials. PbI_2 was purchased from Sigma-Aldrich and dissolved in anhydrous *N*,*N*-dimethylformamide (DMF, from Sigma-Aldrich) with a concentration of 462 mg/mL. CH_3NH_3I was purchased from Lumtec and dissolved in anhydrous 2-propanol (IPA, from Sigma-Aldrich) with a concentration of 35 mg/mL. $PC_{61}BM$ and PEI (with a molecular weight of 25 000 g/mol) were purchased from Nano-C and Sigma-Aldrich, respectively. The PEI was dissolved in 2-methoxyethanol with a weight concentration of 1%. ZnO was synthesized on the basis of the recipe elsewhere.[32] The as-synthesized ZnO nanoparticles were dissolved in chloroform after washing with methanol several times. The concentration of the ZnO solution is

DOI: 10.1021/acsami.5b04695
ACS Appl. Mater. Interfaces 2015, 7, 19986−19993

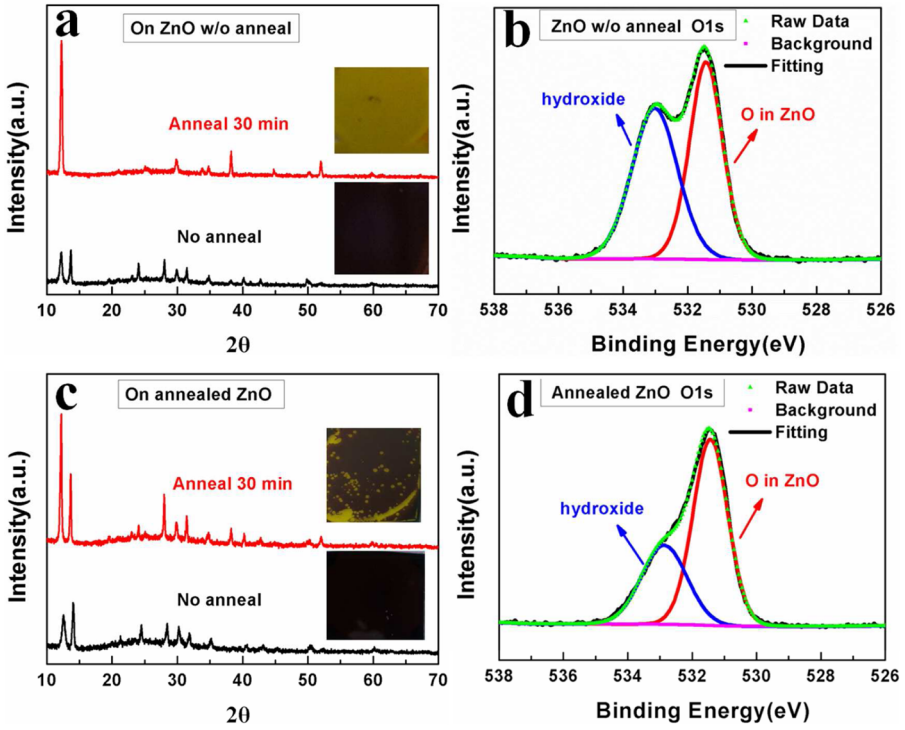

Figure 2. (a) XRD patterns and photographs of perovskite film on ZnO (without annealing) without thermal annealing and annealing at 100 °C for 30 min; high-resolution of O 1s XPS core level spectra of ZnO (b) without annealing and (d) with annealing at 200 °C for 1 h in air. (c) XRD patterns and photographs of perovskite film on annealed ZnO without thermal annealing and annealing at 100 °C for 30 min.

50 mg/mL. The spiro-OMeTAD powder was purchased from Front Materials Co. Ltd. All the chemical reagents were used without any further purification.

Device Fabrication without Buffer Layer. The devices were fabricated on the basis of the structure of ITO/ZnO/$CH_3NH_3PbI_3$ perovskite/spiro-OMeTAD/Au. ITO glasses were cleaned by sonication in deionized water, actone, and ethanol for 15 min each, followed by UV ozone treatment for 20 min. A 30 nm thick layer of ZnO-NPs was spin-coated onto the ITO surface at 4000 rpm for 40 s (for comparison, one ZnO layer was fabricated without annealing and another was annealed at 200 °C for 1 h in air). A PbI_2 solution was then spin-coated on the ZnO layer at 4000 rpm for 40 s. After drying for 10 min, a CH_3NH_3I solution was spin-coated at 4000 rpm for 40 s to form the perovskite film. Subsequently, the spiro-OMeTAD based HTL was spin-coated at 4000 rpm for 40 s. Finally, a 100 nm Au electrode was deposited by thermal evaporation at a base pressure of 10^{-7} Torr. To prepare the spiro-OMeTAD solution, 80 mg of spiro-OMeTAD, 28.5 μL of 4-tertbutylpyridine, and 17.5 μL of lithium bis(trifluoromethanesulfonyl)imide (Li-TFSI) solution (520 mg Li-TFSI in 1 mL acetonitrile) were dissolved in 1 mL of chlorobenzene.

Device Fabrication with Buffer Layer. The devices with $PC_{61}BM$ as buffer layer were fabricated on the basis of the structure of ITO/ZnO/$PC_{61}BM$/$CH_3NH_3PbI_3$/spiro-OMeTAD/Au. Devices with PEI as buffer layer were fabricated on the basis of the structure of ITO/ZnO/PEI/$CH_3NH_3PbI_3$/spiro-OMeTAD/Au. For preparing the buffer layer, a 30 nm $PC_{61}BM$ film was cast from a solution with 25 mg/mL in chlorobenzene at 1000 rpm for 40 s and annealed at 120 °C for 30 min. For preparing the 10 nm PEI layer, we spin-coated the 1 wt % PEI solution in 2-methoxyethanol at 4000 rpm for 40 s, and annealed the film at 100 °C for 30 min. To form the $CH_3NH_3PbI_3$ films on the surface of buffer layer, a PbI_2 solution was spin-coated at 4000 rpm for 40 s. After drying for 10 min, a CH_3NH_3I solution was spin-coated at 4000 rpm for 40 s, followed by thermal annealing at 100 °C for different durations.

Characterizations. The transmission electron microscopy (TEM) measurements were carried out with Philips CM 200 FEG, and the scanning electron microscopy (SEM) measurements were conducted with Philips XL30 FEG. The X-ray diffraction (XRD) measurements were performed on a D2 Phaser instrument using Cu Kα (λ = 0.154 nm) radiation. The chemical compositions of ZnO-NPs with and without thermal annealing were characterized by X-ray photoelectron spectroscopy (XPS, VG ESCALAB 220i-XL UHV). The current–voltage (J–V) characteristics of perovskite solar cells were measured using a Keithley 2400 source meter under AM 1.5G illumination at 100 mW/cm^2, and the effective area of the device was 0.12 cm^2.

3. RESULTS AND DISCUSSION

ZnO-NPs with an average diameter of around 5 nm, as shown in Figure S1a, dissolved in chloroform were used to fabricate the ETL on an ITO substrate. As shown in Figure 1a, the photovoltaic devices have a general structure of ITO/ZnO (30 nm)/$CH_3NH_3PbI_3$ perovskite (280–300 nm)/spiro-OMeTAD (100 nm)/Au. The perovskite films were prepared via two-step spin-coating procedure; details of the fabrication processes are discussed in the Experimental Section.

Figure 1b shows the current density–voltage (J–V) characteristics of the perovskite solar cell under AM 1.5G illustration at 1 sun, which has an open circuit voltage (V_{oc}) of 0.84 V, short circuit current density (J_{sc}) of 7.3 mA/cm^2, fill factor (FF) of 47.6%, and resulting PCE of 2.9%. It should be noted that no thermal annealing treatment was used during this perovskite device fabrication process, and it has been previously reported that, with the same device fabrication process and device architecture, a PCE as high as 15.7% can be achieved.[33] However, we have found that, using the same reported process without thermal annealing, we can only obtain small perovskite crystals, which might be the main reason for the low efficiency in devices. As shown in Figure 1c, the average grain size of the perovskite is only 117 nm. Such small grain size and large number of grain boundaries definitely have significant recombination of photocurrent and detrimental effect on the

DOI: 10.1021/acsami.5b04695
ACS Appl. Mater. Interfaces 2015, 7, 19986–19993

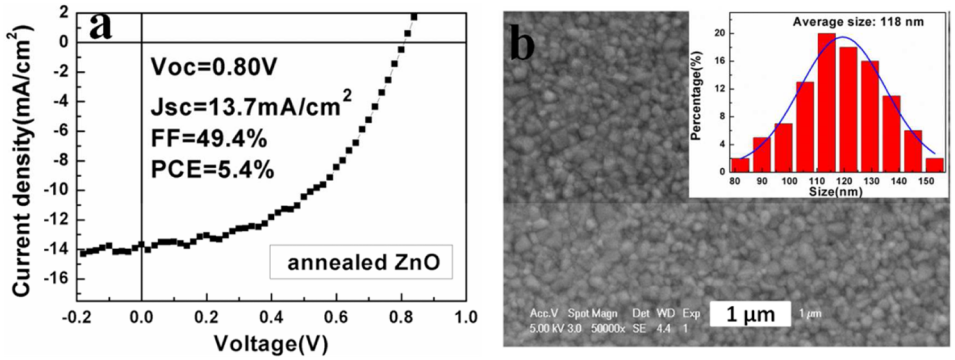

Figure 3. (a) $J-V$ curve of perovskite solar cell based on annealed ZnO; (b) SEM image and grain size distribution of perovskite film (without thermal annealing) deposited on annealed ZnO.

overall device performance. In fact, it has been widely reported that the grain size of perovskite can be increased by thermal annealing; a few hundreds to a few thousands of nanometers of perovskite crystals can be obtained on PEDOT:PSS and TiO_2 layers after being annealed at 100 °C for a long time.[4,5] Surprisingly, as shown in the inset in Figure 2a, the $CH_3NH_3PbI_3$ perovskite film on ZnO-NPs exhibits completely different behavior: it turns from dark brown to yellow even after being annealed at 100 °C just for a few minutes, and the film become completely yellowish in 30 min. This suggests that the $CH_3NH_3PbI_3$ perovskite on ZnO layer could easily decompose into PbI_2 during the thermal annealing process. The decomposition of perovskite crystal was confirmed by the small-angle X-ray diffraction (XRD), and the results were shown in Figure 2a. The diffraction peaks located at 14.1° (110), 28.4° (220), and 42.1° (330) belonged to the $CH_3NH_3PbI_3$ perovskite[9] and diminished after annealing. Meanwhile, the intensity of the diffraction peak at 12.7° that belonged to PbI_2[9] was significantly increased. This indicates that the $CH_3NH_3PbI_3$ perovskite film on ZnO-NP layer completely decomposed into PbI_2 after annealing treatment at 100 °C for 30 min.

In order to gain a deeper insight into the origin of the decomposition of $CH_3NH_3PbI_3$ perovskite on a ZnO-NP layer, we investigated the chemical structure of the ZnO-NP surface by X-ray photoelectron spectroscopy (XPS). As shown in Figure 2b, the O 1s core level spectrum can be resolved into two main peaks located at 531.2 and 530.0 eV, which correspond to the O 1s level in ZnO and other chemisorbed oxygen species such as hydroxide (OH^-) on the surface of the ZnO-NPs, respectively. We speculate that the ZnO was not completely oxidized during the synthesis with the hydrolysis process; thus, the ZnO-NPs may be covered by some chemisorbed oxygen species such as hydroxide on the surface which could break the ionic interaction between $CH_3NH_3^+$ and PbI_3^- and eventually break the crystal structure of perovskite. Here is the proposed reaction route of the decomposition of $CH_3NH_3PbI_3$ promoted by OH^- during thermal annealing:

$$OH^- + CH_3NH_3I \rightarrow CH_3NH_3OH + I^- \quad (1)$$

$$CH_3NH_3OH \xrightarrow{\text{heat}} CH_3NH_2 \uparrow + H_2O\uparrow \quad (2)$$

The OH^- on the surface of ZnO-NPs would react with CH_3NH_3I and form CH_3NH_3OH. Upon annealing, the CH_3NH_3OH would be easily decomposed to CH_3NH_2 and H_2O in the gas phase. Therefore, such reactive process in reaction 2 would promote reaction 1, and consequently lead to the decomposition of $CH_3NH_3PbI_3$ of the reverse process as described in reaction 3:

$$CH_3NH_3I + PbI_2 \Leftrightarrow CH_3NH_3PbI_3 \quad (3)$$

In order to reduce the hydroxide content on the ZnO surface, the ZnO film was annealed at 200 °C for 1 h in air. As shown in Figure 2d, after annealing, the ratio of O in ZnO and O in hydroxide was increased from 1:1 to 2:1, whereas the Zn $2p_{1/2}$ and $2p_{3/2}$ peaks at 1022.5 and 1045.5 eV, respectively, remain the same for ZnO with and without annealing, indicating the Zn exists in the Zn^{2+} state in both samples (Figure S2).

To further confirm the hypothesis that the hydroxide on the surface of ZnO decomposes the $CH_3NH_3PbI_3$ film, we deposited the perovskite film on the annealed ZnO-NP layer. As shown in Figure 2c, after annealing of the perovskite film at 100 °C for 30 min, although there is notable increase of the PbI_2 diffraction peak at 12.7°, the perovskite diffraction peaks located at 14.1°, 28.4°, and 42.1° are also increased. Such reduced decomposition with annealed ZnO is also shown in the inset of Figure 2c; the majority of the perovskite film remains dark brown after annealing, compared to the completely yellowish PbI_2 film on the untreated ZnO. In addition, it should be noted that, even for the perovskite films without annealing, the intensities of $CH_3NH_3PbI_3$ diffraction peaks are stronger than that of the PbI_2 peak for the film deposited on an annealed ZnO-NP layer. This suggests that the formation of $CH_3NH_3PbI_3$ is very sensitive to the hydroxide groups on the ZnO surface.

In addition, we compared the effect of annealing process of perovskite films on both solution processed ZnO-NP thin film and vacuum sputtered ZnO thin film. The hydrolysis-reaction-derived ZnO-NPs prepared in this work have a significantly higher number of OH^- groups compared with that in the sputtered ZnO in vacuum. As shown in Figure S3, after an annealing period of 30 min at 100 °C, there is no notable decomposition of the perovskite film on the sputtered ZnO layer. However, on the ZnO-NP layer, the perovskite film turned to completely yellow, indicating the decomposition of perovskite film. This result confirms our hypothesis that the OH^- groups on the solution derived ZnO-NP surface initiate the decomposition of perovskite.

Furthermore, during the course of submission of this manuscript, Yang et al., by using density functional theory calculations, have reported that the decomposition of the perovskite film at the $ZnO/CH_3NH_3PbI_3$ interface is accelerated by the presence of surface HO^- groups and/or

DOI: 10.1021/acsami.5b04695
ACS Appl. Mater. Interfaces 2015, 7, 19986−19993

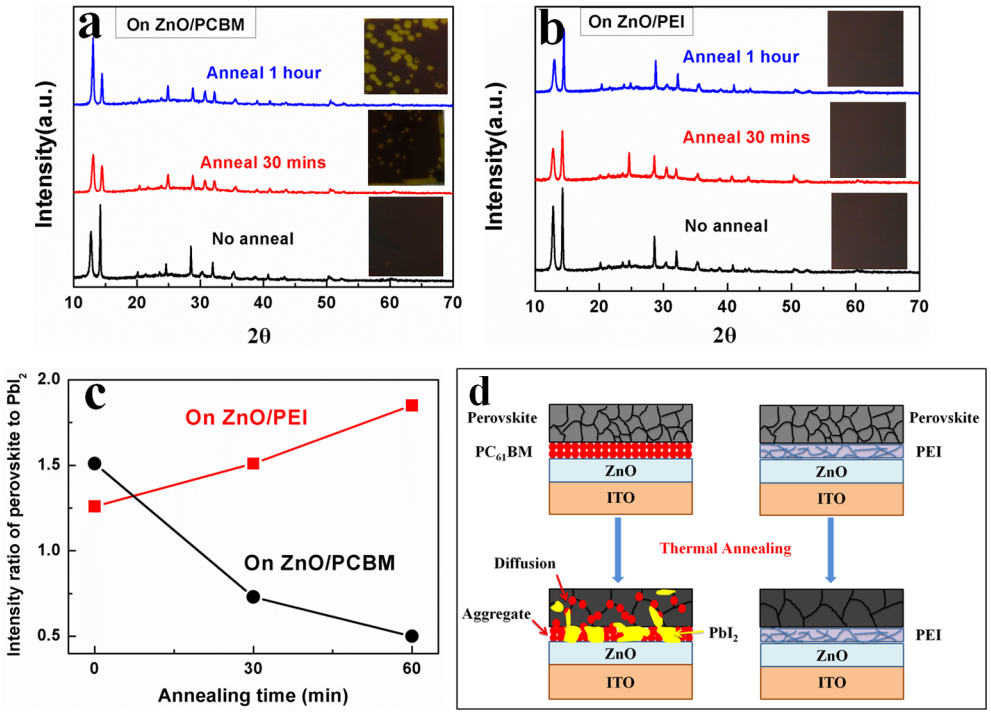

Figure 4. XRD patterns and photographs of perovskite film deposited on (a) $PC_{61}BM$-coated ZnO (b) and PEI-coated ZnO with different thermal annealing treatment, (c) intensity ratio of perovskite to PbI_2 on $PC_{61}BM$-coated ZnO and PEI-coated ZnO, and (d) schematics of the growth of perovskite deposited on $PC_{61}BM$-coated ZnO and PEI-coated ZnO during thermal annealing.

residual acetate ligands.[34] This theoretical result is consistent with our experimental results with the decomposition mechanism as shown in eqs 1 and 2.

To investigate the effect of the content of the hydroxide group in ZnO-NPs on the photovoltaic device performance, we fabricated a perovskite solar cell with annealed ZnO-NPs as the ETL. As shown in Figure 3a, the device had a similar V_{oc} of 0.80 V and FF of 49.4%, but a much higher J_{sc} of 13.7 mA/cm^2, and therefore a larger PCE of 5.4%. As shown in Figure 3b, the average grain size of perovskite on annealed ZnO-NP ETL is around 118 nm, which is similar to that on untreated ZnO NPs. Therefore, the larger J_{sc} is not due to increased grain size but ascribed to the increased amount of $CH_3NH_3PbI_3$ formed on the annealed ZnO surface as shown in the XRD results.

According to the above results, it is clear that the hydroxide groups on ZnO-NP surface promote the decomposition of $CH_3NH_3PbI_3$ to PbI_2 upon thermal annealing. Consequently, it limits the growth of larger $CH_3NH_3PbI_3$ crystals and becomes the major obstacle for developing high-efficiency perovskite solar cell using ZnO as the ETL. As demonstrated below, this issue can be solved by introducing a buffer layer to prevent the perovskite thin film from direct contact with ZnO-NPs. We investigated two buffer layer materials, one based on a small molecule $PC_{61}BM$, and another based on a polymeric PEI. Both materials have been demonstrated with excellent electron transporting properties as an ETL in thin film organic electronic devices.[35,36]

To investigate whether the $PC_{61}BM$ and PEI buffer layers can effectively prevent the perovskite from direct contact with the ZnO layer during the annealing process, $CH_3NH_3PbI_3$ perovskite films were deposited on the $PC_{61}BM$ (30 nm)- and PEI (10 nm)-coated ZnO and annealed at 100 °C. As shown in Figure 4a, the XRD results and optical images of perovskite film with $PC_{61}BM$ as the buffer layer, it can be clearly seen that $PC_{61}BM$ can further reduce but cannot completely avoid the decomposition. The perovskite film in some areas started to turn yellow at 30 min and became larger for 1 h. Furthermore, as shown in Figure 4c, the XRD diffraction peak intensity ratio of perovskite to PbI_2 decreased from 1.51 for no annealing to 0.73 and 0.5 for annealing 30 min and 1 h, respectively. On the other hand, as shown in Figure 4b, the PEI buffer layer showed superb performance to separate the ZnO-NPs and perovskite. The perovskite on PEI-coated ZnO remained dark brown even after annealing for 1 h without notable decomposition of perovskite. This was also confirmed by the XRD results, as shown in Figure 4c: the intensity ratio of perovskite to PbI_2 kept increasing from 1.26 for no annealing to 1.51 and 1.85 for annealing 30 min and 1 h, respectively. For annealing time exceeding 1 h, as shown in Figure S4, the $CH_3NH_3PbI_3$ perovskite started to release CH_3NH_3I, which resulted in a high PbI_2 peak in the XRD measurement.[37] Figure 4d further elucidates the different performances of the two buffer layers. For the small molecule buffer layer, the $PC_{61}BM$ tends to either aggregate or diffuse during the annealing process, which has been widely reported in bulk heterojunction organic solar cells,[38,39] thus leaving the perovskite in contact with the ZnO layer underneath. This agrees with the optical images shown in Figure 4a that the perovskite film started to decompose in certain areas and extended to the whole film upon longer annealing time. Therefore, growing large perovskite crystals in solar cells with $PC_{61}BM$ as the buffer layer is not feasible. On the other hand, the high molecular weight of polymeric PEI is more reluctantly redistributed during the annealing process, which makes it more efficient to prevent the perovskite from contact with the ZnO layer underneath, and it is favorable for the growth of large perovskite crystal during the annealing process.

DOI: 10.1021/acsami.5b04695
ACS Appl. Mater. Interfaces 2015, 7, 19986−19993

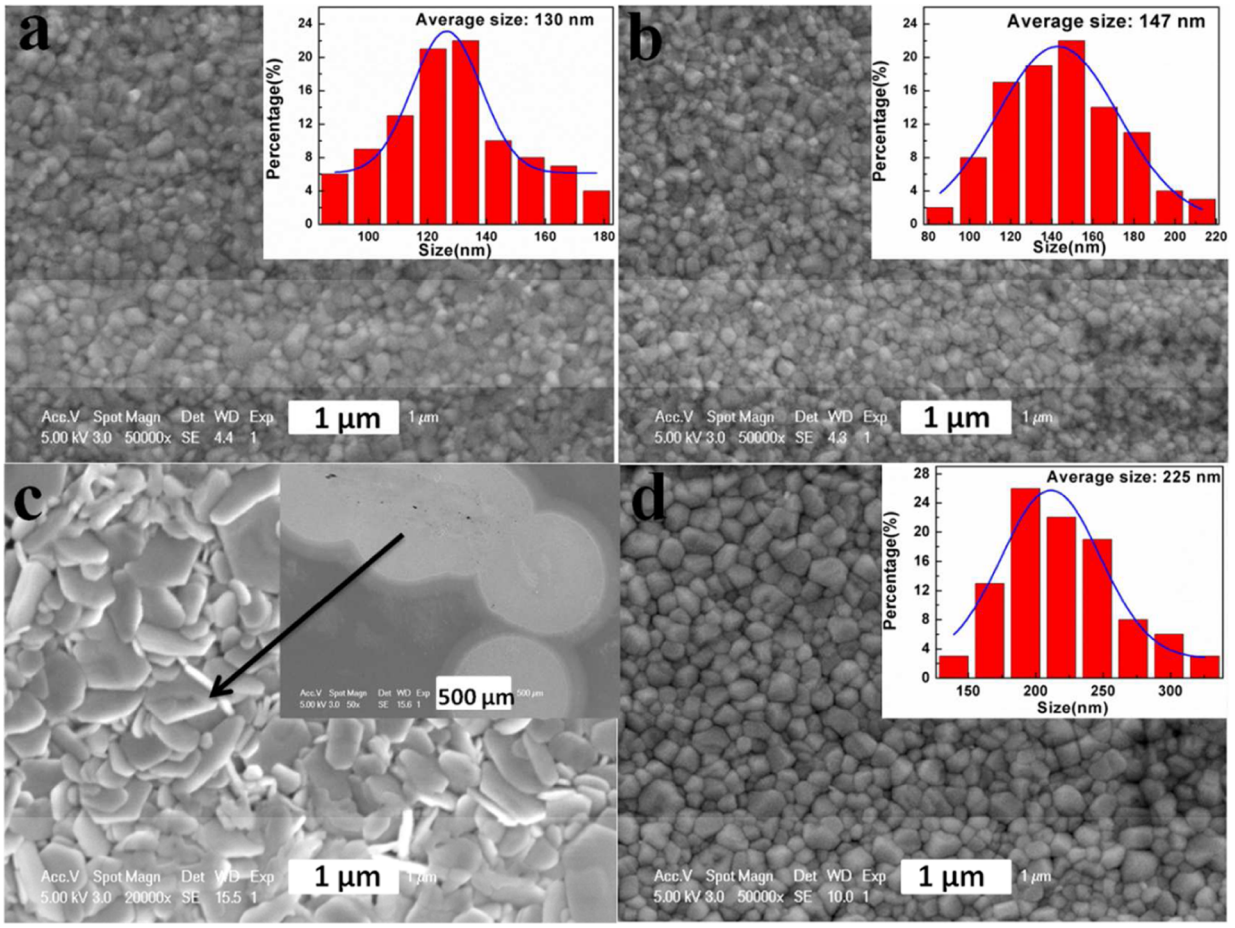

Figure 5. SEM images and grain size distribution of perovskite film deposited on (a) $PC_{61}BM$-coated ZnO without thermal annealing and on PEI-coated ZnO (b) without thermal annealing and (d) with thermal annealing at 100 °C for 1 h. (c) SEM images of perovskite film deposited on $PC_{61}BM$-coated ZnO with thermal annealing at 100 °C.

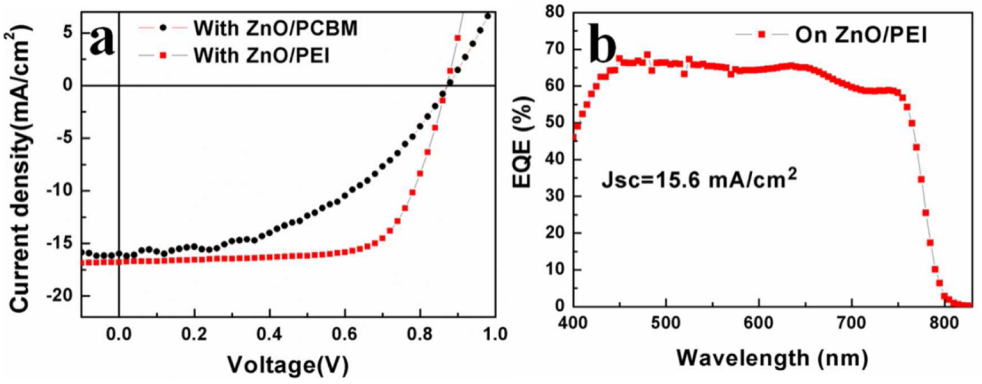

Figure 6. (a) $J-V$ curves of perovskite solar cell based on $PC_{61}BM$-coated and PEI-coated ZnO; (b) EQE spectra of perovskite solar cell based on PEI-coated ZnO.

Figure 5 shows the SEM images of the perovskite film on the top of (a) $PC_{61}BM$- and (b) PEI-coated ZnO. The lateral crystal sizes of perovskite grown on $PC_{61}BM$ and PEI before annealing were similar, with average sizes of 130 and 147 nm, respectively. After annealing the perovskite films at 100 °C for 1 h, as shown in Figure 5c, some large PbI_2 flake crystals were found on the sample using $PC_{61}BM$ as the buffer layer. This is consistent with the XRD results that the PbI_2 diffraction intensity increased after annealing. On the other hand, no such flake crystal was found in perovskite film using PEI as the buffer layer. As shown in Figure 5d, the average lateral size of the perovskite crystal was increased from 147 to 225 nm after annealing.

Figure 6a shows the $J-V$ characteristics of perovskite solar cells using $PC_{61}BM$ and PEI as the buffer layers under AM 1.5G illumination at 100 mW/cm^2. Table 1 summarized the overall solar cell performances of different device structures used in this study. The perovskite solar cell with $PC_{61}BM$ as buffer layer had V_{oc} = 0.88 V, J_{sc} = 16.0 mA/cm^2, FF = 46.0%, and PCE = 6.4%. The device with PEI as the buffer layer had

DOI: 10.1021/acsami.5b04695
ACS Appl. Mater. Interfaces 2015, 7, 19986−19993

Table 1. Photovoltaic Data of Perovskite Solar Cell with Different Buffer Layers

buffer layer	V_{oc} (V)	J_{sc} (mA/cm^2)	FF (%)	PCE (%)
ZnO w/o anneal	0.84	7.3	47.6	2.9
ZnO with anneal	0.80	13.7	49.4	5.4
ZnO/$PC_{61}BM$	0.88	16.0	46.0	6.4
ZnO/PEI	0.88	16.8	69.0	10.2

significant improvement in FF and resulting PCE, with V_{oc} = 0.88 V, J_{sc} = 16.8 mA/cm^2, FF = 69.0%, and PCE = 10.2%. As shown in Figure 6b, the device with PEI as the buffer layer exhibited a broad external quantum efficiency (EQE) from 400 to 800 nm with an integrated J_{sc} of 15.6 mA/cm^2 at AM 1.5G illumination at 100 mW/cm^2, which is in good agreement with the measured $J-V$ characteristics. Compared to the device without buffer layer, with the perovskite films directly spin-coated on the ZnO layer, both devices with buffer layers had better performance, especially in J_{sc}. As demonstrated above, the perovskite film on ZnO will decompose to PbI_2, which has lower light absorption and is relatively electrically insulating; these are the main reasons for the lower J_{sc} in those devices. On the other hand, with PEI as the buffer layer, the perovskite film can be annealed at higher temperature with longer time, and this facilitates the larger perovskite crystal formation with reduced grain boundaries and photocurrent recombination, and therefore improves the FF to 69.0% in photovoltaic device.

Using the ZnO and PEI as the electron transport layer, we fabricated perovskite solar cells on flexible ITO-coated poly(ethylene terephthalate) (PET) substrate, as shown in Figure S5. The flexible device exhibits a V_{oc} of 0.88 V, J_{sc} of 13.76 mA/cm^2, and FF of 62.8%, corresponding to a PCE of 7.6%, and it is still under optimization.

4. CONCLUSIONS

To conclude, we have demonstrated that $CH_3NH_3PbI_3$ perovskite will severely decompose to PbI_2 upon thermal annealing on the ZnO-NP surface. We have found that the hydroxide groups that typically attached on the ZnO-NP surface are the cause of the decomposition process. Two buffer layers, one with small molecular $PC_{61}BM$ and another with polymeric PEI, were investigated to prevent the perovskite from direct contact with ZnO-NP surface. We have found that the decomposition still occurs with $PC_{61}BM$ as the buffer layer, which is mainly due to the aggregation and diffusion of the small molecules during the annealing process. On the other hand, the polymeric buffer layer PEI is more robust which can effectively separate these two materials and allow larger perovksite crystal growth with additional postannealing process. The ZnO based perovskite solar cell using PEI as the buffer layer had significant improvement in fill factor with overall power conversion efficiency over 10%. This work not only demonstrates a route to develop solution processed ZnO based perovskite solar cells for the future development of low-cost applications on flexible substrate, but also presents the importance of the substrate effect on the structural stability and crystal growth of perovskite thin films.

■ ASSOCIATED CONTENT

Supporting Information

The Supporting Information is available free of charge on the ACS Publications website at DOI: 10.1021/acsami.5b04695.

TEM, SEM, XPS, and optical image (PDF)

■ AUTHOR INFORMATION

Corresponding Author

*E-mail: saitsang@cityu.edu.hk.

Author Contributions

Y.C. and Q.-D.Y. contributed equally to this work.

Notes

The authors declare no competing financial interest.

■ ACKNOWLEDGMENTS

This work is supported by Research Grants Council of the Hong Kong Special Administrative Region, China (Project No. 21201514), and CityU start-up grant (CityU-7200372, CityU-9610309) received by Dr. S.-W. Tsang.

■ REFERENCES

(1) Kojima, A.; Teshima, K.; Shirai, Y.; Miyasaka, T. Organometal Halide Perovskites as Visible-Light Sensitizers for Photovoltaic Cells. *J. Am. Chem. Soc.* **2009**, *131*, 6050−6051.

(2) Kim, H.-S.; Lee, C.-R.; Im, J.-H.; Lee, K.-B.; Moehl, T.; Marchioro, A.; Moon, S.-J.; Humphry-Baker, R.; Yum, J.-H.; Moser, J. E.; Gratzel, M.; Park, N.-G. Lead Iodide Perovskite Sensitized All-Solid-State Submicron Thin Film Mesoscopic Solar Cell with Efficiency Exceeding 9%. *Sci. Rep.* **2012**, *2*, 591.

(3) *Research Cell Efficiency Records*; NREL, http://www.nrel.gov/ncpv/images/efficiency_chart.jpg. Accessed on December 9, 2014.

(4) Zhou, H.; Chen, Q.; Li, G.; Luo, S.; Song, T.-b.; Duan, H.-S.; Hong, Z.; You, J.; Liu, Y.; Yang, Y. Interface Engineering of Highly Efficient Perovskite Solar Cells. *Science* **2014**, *345*, 542−546.

(5) Im, J.-H.; Jang, I.-H.; Pellet, N.; Gratzel, M.; Park, N.-G. Growth of CH3NH3PbI3 Cuboids with Controlled Size for High-efficiency Perovskite Solar Cells. *Nat. Nanotechnol.* **2014**, *9*, 927−932.

(6) Nie, W.; Tsai, H.; Asadpour, R.; Blancon, J.-C.; Neukirch, A. J.; Gupta, G.; Crochet, J. J.; Chhowalla, M.; Tretiak, S.; Alam, M. A.; Wang, H.-L.; Mohite, A. D. High-efficiency Solution-processed Perovskite Solar Cells with Millimeter-scale Grains. *Science* **2015**, *347*, 522−525.

(7) Heo, J. H.; Han, H. J.; Kim, D.; Ahn, T. K.; Im, S. H. Hysteresis-less Inverted $CH_3NH_3PbI_3$ Planar Perovskite Hybrid Solar Cells with 18.1% Power Conversion Efficiency. *Energy Environ. Sci.* **2015**, *8*, 1602−1608.

(8) Juarez-Perez, E. J.; Wuβler, M.; Fabregat-Santiago, F.; Lakus-Wollny, K.; Mankel, E.; Mayer, T.; Jaegermann, W.; Mora-Sero, I. Role of the Selective Contacts in the Performance of Lead Halide Perovskite Solar Cells. *J. Phys. Chem. Lett.* **2014**, *5*, 680−685.

(9) Zhao, D.; Sexton, M.; Park, H.-Y.; Baure, G.; Nino, J. C.; So, F. High-Efficiency Solution-Processed Planar Perovskite Solar Cells with a Polymer Hole Transport Layer. *Adv. Energy Mater.* **2015**, *5*, 1401855−1401859.

(10) Lloyd, M. T.; Olson, D. C.; Lu, P.; Fang, E.; Moore, D. L.; White, M. S.; Reese, M. O.; Ginley, D. S.; Hsu, J. W. P. Impact of Contact Evolution on the Shelf Life of Organic Solar Cells. *J. Mater. Chem.* **2009**, *19*, 7638−7642.

(11) Voroshazi, E.; Verreet, B.; Buri, A.; Müller, R.; Nuzzo, D. D.; Heremans, P. Influence of Cathode Oxidation via the Hole Extraction Layer in Polymer: Fullerene Solar Cells. *Org. Electron.* **2011**, *12*, 736−744.

(12) Jeon, N. J.; Noh, J. H.; Yang, W. S.; Kim, Y. C.; Ryu, S.; Seo, J.; Seok, S. I. Compositional Engineering of Perovskite Materials for High-performance Solar Cells. *Nature* **2015**, *517*, 476−480.

(13) Ye, S.; Sun, W.; Li, Y.; Yan, W.; Peng, H.; Bian, Z.; Liu, Z.; Huang, C. CuSCN-Based Inverted Planar Perovskite Solar Cell with an Average PCE of 15.6%. *Nano Lett.* **2015**, *15*, 3723−3728.

(14) Kim, J. H.; Liang, P. W.; Williams, S. T.; Cho, N.; Chueh, C. C.; Glaz, M. S.; Ginger, D. S.; Jen, A. K.-Y. High-Performance and Environmentally Stable Planar Heterojunction Perovskite Solar Cells Based on a Solution-Processed Copper-Doped Nickel Oxide Hole-Transporting Layer. *Adv. Mater.* **2015**, *27*, 695−701.

DOI: 10.1021/acsami.5b04695
ACS Appl. Mater. Interfaces 2015, 7, 19986−19993

(15) Zhao, Y.; Nardes, A. M.; Zhu, K. Solid-State Mesostructured Perovskite $CH_3NH_3PbI_3$ Solar Cells: Charge Transport, Recombination, and Diffusion Length. *J. Phys. Chem. Lett.* **2014**, *5*, 490−494.
(16) Moehl, T.; Im, J. H.; Lee, Y.; Domanski, K.; Giordano, F.; Zakeeruddin, S. M.; Dar, M. I.; Heiniger, L.-P.; Nazeeruddin, M. K.; Park, N.-G.; Gratzel, M. Strong Photocurrent Amplification in Perovskite Solar Cells with a Porous TiO_2 Blocking Layer under Reverse Bias. *J. Phys. Chem. Lett.* **2014**, *5*, 3931−3936.
(17) Dong, J.; Zhao, Y.; Shi, J.; Wei, H.; Xiao, J.; Xu, X.; Luo, J.; Xu, J.; Li, D.; Luo, Y.; Meng, Q. Impressive Enhancement in the Cell Performance of ZnO Nanorod-based Perovskite Solar Cells with Al-doped ZnO Interfacial Modification. *Chem. Commun.* **2014**, *50*, 13381−13384.
(18) Ke, W.; Fang, G.; Liu, Q.; Xiong, L.; Qin, P.; Tao, H.; Wang, J.; Lei, H.; Li, B.; Wan, J.; Yang, G.; Yan, Y. Low-Temperature Solution-Processed Tin Oxide as an Alternative Electron Transporting Layer for Efficient Perovskite Solar Cells. *J. Am. Chem. Soc.* **2015**, *137*, 6730−6733.
(19) Green, M. A.; Ho-Baillie, A.; Snaith, H. J. The Emergence of Perovskite Solar Cells. *Nat. Photonics* **2014**, *8*, 506−514.
(20) Hayashi, H.; Lightcap, I. V.; Tsujimoto, M.; Takano, M.; Umeyama, T.; Kamat, P. V.; Imahori, H. Electron Transfer Cascade by Organic/Inorganic Ternary Composites of Porphyrin, Zinc Oxide Nanoparticles, and Reduced Graphene Oxide on a Tin Oxide Electrode that Exhibits Efficient Photocurrent Generation. *J. Am. Chem. Soc.* **2011**, *133*, 7684−7687.
(21) Alem, S.; Lu, J.; Movileanu, R.; Kololuoma, T.; Dadvand, A.; Tao, Y. Solution-processed Annealing-free ZnO Nanoparticles for Stable Inverted Organic Solar Cells. *Org. Electron.* **2014**, *15*, 1035−1042.
(22) Sun, Y.; Seo, J. H.; Takacs, C. J.; Seifter, J.; Heeger, A. J. Inverted Polymer Solar Cells Integrated with a Low-Temperature-Annealed Sol-Gel-Derived ZnO Film as an Electron Transport Layer. *Adv. Mater.* **2011**, *23*, 1679−1683.
(23) Chen, S.; Manders, J. R.; Tsang, S.-W.; So, F. Metal Oxides for Interface Engineering in Polymer Solar Cells. *J. Mater. Chem.* **2012**, *22*, 24202−24212.
(24) Small, C. E.; Chen, S.; Subbiah, J.; Amb, C. M.; Tsang, S.-W.; Lai, T.-H.; Reynolds, J. R.; So, F. High-efficiency Inverted Dithienogermole-thienopyrrolodione-based Polymer Solar Cells. *Nat. Photonics* **2012**, *6*, 115−120.
(25) You, J.; Dou, L.; Yoshimura, K.; Kato, T.; Ohya, K.; Moriarty, T.; Emery, K.; Chen, C.-C.; Gao, J.; Li, G.; Yang, Y. A Polymer Tandem Solar Cell with 10.6% Power Conversion Efficiency. *Nat. Commun.* **2013**, *4*, 1446−1455.
(26) Ball, J. M.; Lee, M. M.; Hey, A.; Snaith, H. J. Low-temperature Processed Meso-superstructured to Thin-film Perovskite Solar Cells. *Energy Environ. Sci.* **2013**, *6*, 1739−1743.
(27) Song, X.; Wang, W.; Sun, P.; Ma, W.; Chen, Z.-K. Additive to Regulate the Perovskite Crystal Film Growth in Planar Heterojunction Solar Cells. *Appl. Phys. Lett.* **2015**, *106*, 033901−033905.
(28) Snaith, H. J.; Abate, A.; Ball, J. M.; Eperon, G. E.; Leijtens, T.; Noel, N. K.; Stranks, S. D.; Wang, J. T.-W.; Wojciechowski, K.; Zhang, W. Anomalous Hysteresis in Perovskite Solar Cells. *J. Phys. Chem. Lett.* **2014**, *5*, 1511−1515.
(29) Ip, A. H.; Quan, L. N.; Adachi, M. M.; McDowell, J. J.; Xu, J.; HaKim, D.; Sargent, E. H. A Two-step Route to Planar Perovskite Cells Exhibiting Reduced Hysteresis. *Appl. Phys. Lett.* **2015**, *106*, 143902−143906.
(30) Kumar, M. H.; Yantara, N.; Dharani, S.; Graetzel, M.; Mhaisalkar, S.; Boix, P. P.; Mathews, N. Flexible, Low-temperature, Solution Processed ZnO-based Perovskite Solid State Solar Cells. *Chem. Commun.* **2013**, *49*, 11089−11091.
(31) Son, D.-Y.; Im, J.-H.; Kim, H.-S.; Park, N.-G. 11% Efficient Perovskite Solar Cell Based on ZnO Nanorods: An Effective Charge Collection System. *J. Phys. Chem. C* **2014**, *118*, 16567−16573.
(32) Beek, W. J. E.; Wienk, M. M.; Kemerink, M.; Yang, X.; Janssen, R. A. J. Hybrid Zinc Oxide Conjugated Polymer Bulk Heterojunction Solar Cells. *J. Phys. Chem. B* **2005**, *109*, 9505−9516.
(33) Liu, D.; Kelly, T. L. Perovskite Solar Cells with a Planar Heterojunction Structure Prepared Using Room-temperature Solution Processing Techniques. *Nat. Photonics* **2014**, *8*, 133−138.
(34) Yang, J.; Siempelkamp, B. D.; Mosconi, E.; Angelis, F. D.; Kelly, T. L. Origin of the Thermal Instability in $CH_3NH_3PbI_3$ Thin Films Deposited on ZnO. *Chem. Mater.* **2015**, *27*, 4229−4236.
(35) Shivanna, R.; Shoaee, S.; Dimitrov, S.; Kandappa, S. K.; Rajaram, S.; Durrant, J. R.; Narayan, K. S. Charge Generation and Transport in Efficient Organic Bulk Heterojunction Solar Cells with a Perylene Acceptor. *Energy Environ. Sci.* **2014**, *7*, 435−441.
(36) Woo, S.; Kim, W. H.; Kim, H.; Yi, Y.; Lyu, H.-K.; Kim, Y. 8.9% Single-Stack Inverted Polymer Solar Cells with Electron-Rich Polymer Nanolayer-Modified Inorganic Electron-Collecting Buffer Layers. *Adv. Energy Mater.* **2014**, *4*, 1301692−1301698.
(37) Chen, Q.; Zhou, H.; Song, T.-B.; Luo, S.; Hong, Z.; Duan, H.-S.; Dou, L.; Liu, Y.; Yang, Y. Controllable Self-Induced Passivation of Hybrid Lead Iodide Perovskites toward High Performance Solar Cells. *Nano Lett.* **2014**, *14*, 4158−4163.
(38) Treat, N. D.; Shuttle, C. G.; Toney, M. F.; Hawker, C. J.; Chabinyc, M. L. In Situ Measurement of Power Conversion Efficiency and Molecular Ordering during Thermal Annealing in P_3HT:PCBM Bulk Heterojunction Solar Cells. *J. Mater. Chem.* **2011**, *21*, 15224−15231.
(39) Treat, N. D.; Brady, M. A.; Smith, G.; Toney, M. F.; Kramer, E. J.; Hawker, C. J.; Chabinyc, M. L. Interdiffusion of PCBM and P_3HT Reveals Miscibility in a Photovoltaically Active Blend. *Adv. Energy Mater.* **2011**, *1*, 82−89.

NOTE ADDED AFTER ASAP PUBLICATION

This paper was published ASAP on August 24, 2015. The image in Figure 2 was replaced, the text in the Results and Discussion section was modified, and the revised version was reposted on September 1, 2015.

DOI: 10.1021/acsami.5b04695
ACS Appl. Mater. Interfaces 2015, 7, 19986−19993